32. Mandell GA, Harcke HT, Sharkey C, Brooks KM, MacEwen GD. SPECT imaging of para-axial neurofibromatosis with ^{99m}Tc DTPA. *J Nucl Med* 1987;28:1688–1694.
33. Mandell GA, Herrick WC, Harcke HT, Sharkey C, Brooks KM, MacEwen GD. Neurofibromas: location by scanning with ^{99m}Tc-DTPA. Work in progress. *Radiology* 1985;157:803–806.
34. Abdel-Dayem HM, Papademetriou T. Subperiosteal hemorrhage in neurofibromatosis: appearance in bone scintigraphy. *Clin Nucl Med* 1981;6:272.
35. Ohta H, Endo K, Fujita T, et al. Imaging of soft tissue tumors with ^{99m}Tc(V) dimercaptosuccinic acid. A new tumor-seeking agent. *Clin Nucl Med* 1984;9:568–573.
36. Kobayashi H, Kotoura Y, Sakahara H, et al. Schwannoma of the extremities: comparison of MRI and pentavalent technetium-99m-dimercaptosuccinic acid and gallium-67-citrate scintigraphy. *J Nucl Med* 1994;35:1174–1178.
37. Wilkinson RH Jr., Goodrich JK. A neurofibroma mimicking a parotid gland tumor both clinically and by scanning. *J Nucl Med* 1971;12:646–648.
38. Koch KJ, Siddiqui AR, Wellman HN, Campbell RL. Localization of technetium-99m pertechnetate in peripheral nerve tumors. *J Nucl Med* 1986;27:1713–1716.
39. Grove AS Jr., Kotner LM Jr. Orbital scanning with multiple radionuclides. *Arch Ophthalmol* 1973;89:301–305.
40. Siddiqui AR. Localization of technetium-99m DTPA in neurofibroma [Letter]. *J Nucl Med* 1986;27:143–144.
41. Mandell GA, Scott CI Jr., Harcke HT, Sharkey C, Harris L. Scintigraphic differentiation of congenital soft-tissue extremity enlargement with ^{99m}Tc-DTPA. *Skeletal Radiol* 1989;18:33–41.
42. Goshen E, Meller I, Lantsberg S, et al. Radionuclide imaging of soft tissue masses with ^{99m}Tc-DTPA. *Clin Nucl Med* 1991;16:636–642.
43. Ida M, Mashima Y, Mori Y, Kawakami K, Kondoh H. Evaluation of ^{99m}Tc-DTPA as tumor seeking agents for neurofibromatosis. *Kaku Igaku* 1988;25:205–212.
44. Sty JR, Starshak RJ, Woods GA. Neurofibromatosis: lymphoscintigraphic observations. *Clin Nucl Med* 1981;6:264–265.
45. Hammond JA, Driedger AA. Detection of malignant change in neurofibromatosis (von Recklinghausen's disease) by gallium-67 scanning. *Can Med Assoc J* 1978;119:352–353.
46. Wang PW, Chen HY, Li CH, Chen WJ. Uptake of ^{131}I by an abdominal neurilemoma mimicking metastatic thyroid carcinoma. *Clin Nucl Med* 1993;18:964–966.
47. Kalff V, Shapiro B, Lloyd R, et al. The spectrum of pheochromocytoma in hypertensive patients with neurofibromatosis. *Arch Intern Med* 1982;142:2092–2098.
48. Von Moll L, McEwan AJ, Shapiro B, et al. Iodine-131 MIBG scintigraphy of neuroendocrine tumors other than pheochromocytoma and neuroblastoma. *J Nucl Med* 1987;28:979–988.
49. Borbely K, Fulham MJ, Brooks RA, Di Chiro G. PET-fluorodeoxyglucose of cranial and spinal neuromas. *J Nucl Med* 1992;33:1931–1934.
50. Young DF, Eldridge R, Gardner WJ. Bilateral acoustic neuroma in a large kindred. *JAMA* 1970;214:347–353.
51. Baker ND, Tchang FK, Greenspan A. Liposarcoma complicating neurofibromatosis. Report of two cases. *Bull Hosp Jt Dis Orthop Inst* 1982;42:172–186.

Quantitative Comparison of Planar and SPECT Normal Data Files of Thallium-201, Technetium-99m-Sestamibi, Technetium-99m-Tetrofosmin and Technetium-99m-Furifosmin

Hitoshi Naruse, Edouard Daher, Albert Sinusas, Diwakar Jain, Donna Natale, Jennifer Mattera, Robert Makuch and Frans J.Th. Wackers

The Cardiovascular Nuclear Imaging Laboratory, Departments of Diagnostic Radiology, Medicine, Epidemiology and Public Health, Yale University School of Medicine, New Haven, Conneticut

In recent years, several of ^{99m}Tc-labeled myocardial perfusion imaging agents have been developed, such as ^{99m}Tc-sestamibi, ^{99m}Tc-tetrofosmin and ^{99m}Tc-furifosmin. Although images obtained with these new tracers have a general similar appearance, there are differences in the myocardial kinetics, body distribution, general quality of images and imaging protocols. The aim of this study was to quantitatively compare normal exercise planar and SPECT data files obtained with ^{201}Tl and ^{99m}Tc-labeled agents. **Methods:** Lower-limit-of-normal curves were generated for each specific radiopharmaceutical from normal subjects with low (<3%) pretest likelihood of coronary artery disease using circumferential count distribution profiles from planar and SPECT exercise images. Lower-limit-of-normal curves were statistically compared using the nonparametric Kruskall-Wallis and Wilcoxon tests. **Results:** Planar and SPECT lower-limit-of-normal curves generated for each radiopharmaceutical showed general similarities. Statistically significant differences among the lower-limit-of-normal curves were found in the planar left anterior oblique view and in the planar left lateral view ($p < 0.05$ for each). No statistically significant differences existed between lower-limit-of-normal curves of various radiopharmaceuticals on the planar anterior view and on SPECT imaging **Conclusion:** For quantitative analysis of planar images, radiopharmaceutical-specific normal data files are mandatory. Although SPECT normal data files of various radiopharmaceuticals are not statistically different, they are not identical. It appears, nevertheless, prudent to use radiopharmaceutical-specific normal data files for quantitative analysis of SPECT images.

Key Words: normal data files; quantification; thallium-201; sestamibi; tetrofosmin; furifosmin.

J Nucl Med 1996; 37:1783–1788

Received Dec. 5, 1995; revision accepted Mar. 22, 1996.

For correspondence or reprints contact: Frans J.Th. Wackers, MD, Cardiovascular Nuclear Imaging and Exercise Laboratories, Yale University School of Medicine, 333 Cedar St. (TE-2) P.O. Box 208042, New Haven, CT 06520-8042.

Several new radiopharmaceuticals have been introduced in recent years for stress myocardial perfusion imaging. Because of unfavorable characteristics of the conventional imaging agent, ^{201}Tl (*1*), ^{99m}Tc-labeled agents with better imaging properties have been developed such as ^{99m}Tc-sestamibi (*2*), ^{99m}Tc-tetrofosmin (*3*) and ^{99m}Tc-furifosmin (*4*). These new radiopharmaceuticals provide improved image quality, particularly when used for SPECT. Normal images with each of the above imaging agents, using either planar or SPECT imaging, have visually a similar general appearance i.e., more or less homogeneous myocardial uptake. Nevertheless, there are marked differences in myocardial kinetics, body distribution, general quality of images and imaging protocols (*2,3,5–7*).

Quantification of planar and SPECT images enhances confidence and reproducibility of image interpretation (*8–10*). In addition, quantitative measurement of myocardial perfusion abnormalities has shown to be of importance for prognostic risk stratification in individual patients (*11–13*). The most important components of image quantification are graphic or color-coded display of relative myocardial radiopharmaceutical distribution and normal data files for comparison with patient image data (*9,14*).

TABLE 1
Subject Characteristics Included in Planar and SPECT Normal Data Files

Agent	No. of normal subjects	Age (yr) (m + s.d.)	Age (yr) (range)	Sex (% Male)	Weight (lb)
Planar					
Thallium	26	35 ± 13	na	62	na
Sestamibi	20	35 ± 9	na	70	na
Tetrofosmin	27	37 ± 8	24–55	68	155 ± 18
Furifosmin	22	30 ± 11	19–54	75	158 ± 20
SPECT					
Thallium	26	33 ± 12	na	62	na
Sestamibi	13	37 ± 9	na	76	na
Tetrofosmin	42	38 ± 10	24–63	63	159 ± 21
Furifosmin	25	31 ± 9	19–54	67	160 ± 25

m ± s.d. = mean ± standard deviation; na = data not acquired or available.

The purpose of the present study was to compare quantitatively planar and SPECT normal exercise image data files obtained with ^{201}Tl, ^{99m}Tc-sestamibi, ^{99m}Tc-tetrofosmin and ^{99m}Tc-furifosmin.

MATERIALS AND METHODS

Patients

Normal exercise data files for each radiopharmaceutical were generated by imaging normal subjects after exercise. The normal data files were acquired over a period of 13 yr, initially for ^{201}Tl. However, when new imaging agents were later introduced, normal data files were acquired for each of these new radiopharmaceuticals. Consequently, the normal subjects imaged with various radiopharmaceuticals were not always the same individuals. Although some individuals had both planar and SPECT imaging, the normal data files for each imaging modality were generally not derived from the same individuals.

For planar imaging, normal data files of ^{201}Tl, sestamibi, tetrofosmin and furifosmin were derived from 26, 20, 27 and 22 subjects, respectively. For SPECT imaging, normal data files of ^{201}Tl, sestamibi, tetrofosmin and furifosmin were derived from 26, 13, 42 and 25 subjects, respectively. The normal subjects were volunteers, who, to be included in the normal data files, had to meet the following inclusion criteria: (a) less than 3% pretest likelihood of having coronary artery disease based upon absence of symptoms, age, gender, physical examination and normal rest-exercise electrocardiogram (*15*), (b) visually images without artifacts, i.e. images of women with obvious breast attenuation artifacts and images of subjects with motion artifacts or severe diaphragmatic attenuation were excluded and (c) adequate technical image quality. The images all had adequate count density, i.e., at least 35k counts in the background corrected left ventricle on planar images and at least 100 counts in the hottest pixel of the left ventricle on an anterior projection image for SPECT imaging. The age, gender and weights of these subjects are shown in Table 1. No subject weighed more than 200 lb. Informed consent was obtained from all normal subjects.

Exercise

All patients performed symptom-limited treadmill exercise using the standard Bruce protocol. Endpoints for exercise were attainment of 85% of age-predicted maximal heart rate. The radiopharmaceutical was injected at peak exercise and exercise was continued for another 1–2 min.

Radiopharmaceutical Dose and Imaging Protocols

Thallium-201. At peak exercise, 2.0–3.5 mCi (74–130 MBq) of ^{201}Tl were injected. Imaging was started within 5 min after termination of exercise for planar imaging and at 10 min after exercise for SPECT imaging.

Technetium-99m-Sestamibi. At peak exercise, approximately 30 mCi (1110 MBq) ^{99m}Tc-sestamibi were injected. Imaging was started 30–60 min after termination of exercise for both planar and SPECT imaging.

Technetium-99m-Tetrofosmin. At peak exercise, approximately 8 mCi ^{99m}Tc-tetrofosmin were injected. Imaging was started 20–40 min after termination of exercise for both planar and SPECT imaging.

Technetium-99m-Furifosmin. At peak exercise, approximately 10 mCi ^{99m}Tc-furifosmin were injected. Imaging was started 20–40 min after termination of exercise for both planar and SPECT imaging.

Equipment

Imaging was performed using standard planar and SPECT gamma cameras. Low-energy, all-purpose collimation was used for planar and SPECT ^{201}Tl imaging; low-energy, high-resolution collimation was used for planar and SPECT imaging of ^{99m}Tc-labeled compounds. The energy window (20%) was centered symmetrically over the 68–80-keV mercury x-rays of ^{201}Tl and over the 140-keV photopeak of ^{99m}Tc.

Planar Imaging and Image Processing

Planar myocardial perfusion images were acquired in three views: supine anterior view, supine left anterior oblique view and right side decubitus left lateral view. Images were acquired for 8 min (^{201}Tl) and 5 min (^{99m}Tc-agents) on the computer using a 128 × 128 matrix (word mode). After modified interpolative background subtraction (*16*), circumferential count distribution profiles were generated for quantification of relative myocardial radiopharmaceutical distribution (*14,16–19*).

SPECT Imaging and Image Processing

For SPECT imaging, 32 projection images were acquired over a 180° arc, from right anterior oblique to left posterior oblique. Time per stop was 40 sec for ^{201}Tl and 20 sec and 40 sec for high-dose

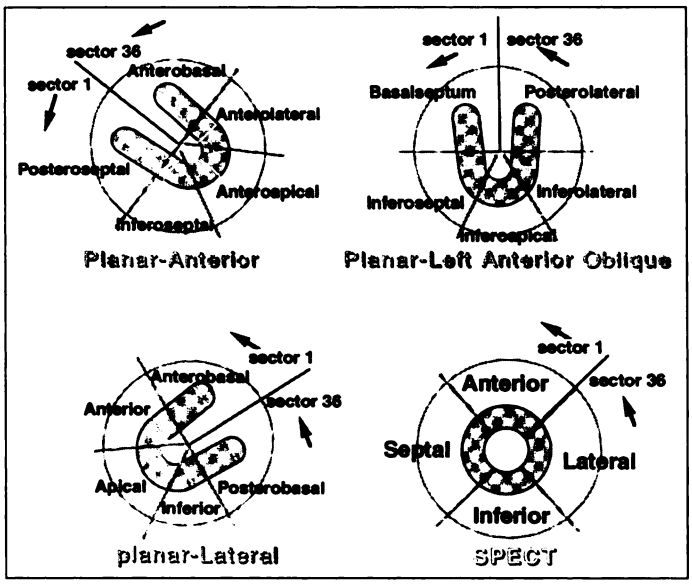

FIGURE 1. Anatomic segments on three planar and short axis SPECT myocardial perfusion images. Each image is divided in 36 sectors for generation of circumferential count distribution profiles.

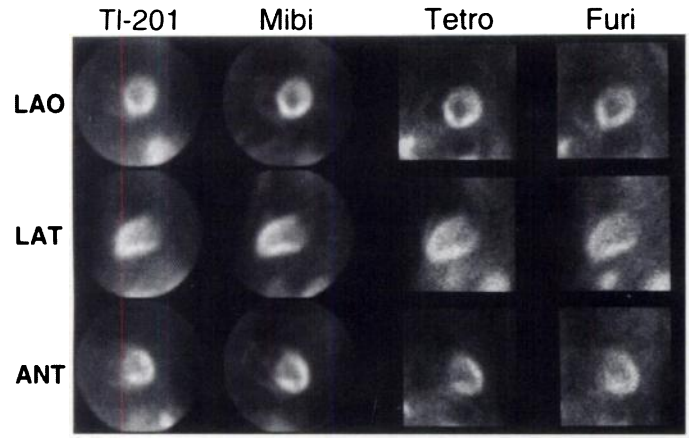

FIGURE 2. Representative planar images with ^{201}Tl, ^{99m}Tc-sestamibi (Mibi), ^{99m}Tc-tetrofosmin (Tetro) and ^{99m}Tc-furifosmin (Furi). All images are from the same normal subject.

and low-dose ^{99m}Tc-labeled agents, respectively. SPECT images were acquired on a computer using 64 × 64 matrix and stored on either a floppy or optical disks. The projection images were processed using a low-pass (Butterworth) filter, with an order of 4.0 and a cutoff of 0.22 cycles/pixel for ^{201}Tl and a cutoff of 0.25 cycles/pixel for ^{99m}Tc. Subsequently, standard backprojection using a ramp filter was performed. Tomographic slices (approximately 6 mm thick) were reconstructed relative to anatomical axis of the left ventricle. Vertical and horizontal long-axis slices and the short-axis slices were generated. For quantification, circumferential count distribution profiles were generated from the apical through basal short-axis slices.

Image Quantification and Generation of Circumferential Profiles

Relative myocardial distribution of radiopharmaceutical accumulation was quantified by generating circumferential count distribution profiles (*14,17–19*). The left ventricle on the background-corrected (*16*) planar images and on the reconstructed SPECT short-axis slices was divided in 36 sectors (Fig. 1). For planar imaging, average counts per sector, and for SPECT imaging, maximal counts per sector, were displayed relative to the sectors with maximal absolute counts, which was assigned a value of 100%. For planar imaging three circumferential profile are generated, one for each planar image (anterior, left anterior oblique and left lateral). For SPECT imaging circumferential profiles were generated of only those short axis slices showing circular full-

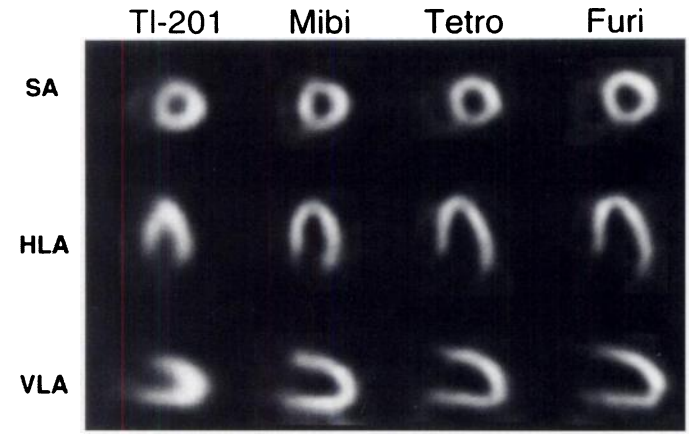

FIGURE 3. Representative SPECT images with ^{201}Tl, ^{99m}Tc-sestamibi (Mibi), ^{99m}Tc-tetrofosmin (Tetro) and ^{99m}Tc-furifosmin (Furi) in normal subjects. The ^{201}Tl and Mibi images are from the same normal subject, the Tetro and Furi images are from two different normal individuals.

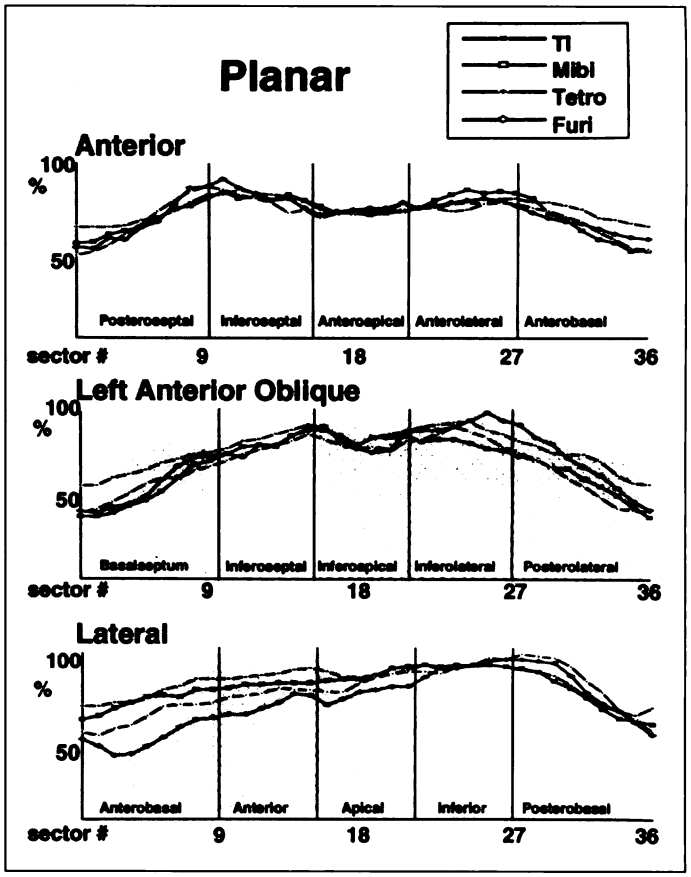

FIGURE 4. Lower-limit-of-normal curves of four radiopharmaceuticals in planar anterior, left anterior oblique and left lateral views. Shaded segments indicate statistically significant differences among the curves of various radiopharmaceuticals (see text).

thickness myocardium: apical short-axis slices without definite left ventricular cavity and basal slices with the membranous septum were excluded. The remaining short-axis slices, the number of which may vary depending on the size of the heart in individual patients, were interpolated to nine slices: three apical, three midventricular and three basal slices. Circumferential count profiles were generated for each of the nine slices. To simplify the statistical analysis, the three circumferential profiles of the apical, midventricular and basal left ventricular regions were averaged.

Generation of Normal Image Data Files

For each of 36 data points of the circumferential profiles of normal subjects, the mean and s.d. was determined for each radiopharmaceutical and for each imaging technique. Circumferential profiles of male and female subjects were averaged together. The lower-limit-of-normal myocardial radiopharmaceutical distribution was defined as "mean minus 2 s.d.". By using this quantitative method, we obtained sensitivity, specificity and normalcy rates of 89%, 95% and 97%, respectively for planar imaging, and 92%, 80% and 100% for SPECT imaging.

For statistical analysis, the circumferential profile data points were grouped into five anatomic segments on planar images and into four anatomic segments on SPECT images.

Statistical Comparison of Normal Data Files

The Wilks-Sharpiro test was used to statistically examine the distributional assumption of normality of data. Whereas mean data often departed from normality, mean − 2 s.d. data rarely departed from normality based on the Wilks-Shapiro test. Using means as a measure of central tendency, as well as for ease of data display to present and analyze the mean − 2 s.d. data.

TABLE 2
Statistical Analysis of Paired Lower-Limit-of-Normal Curves in Planar Left Anterior Oblique View and Planar Left Lateral View Using the Wilcoxon Test

	Planar left anterior oblique view					
	Comparison of two curves (p-value)					
Anatomic region	Tl vs. Mibi	Tl vs. Tetro	Tl vs. Furi	Mibi vs. Tetro	Mibi vs. Furi	Tetro vs. Furi
Basalseptum	*	*	ns	ns	ns	ns
Inferoseptal	ns	ns	ns	ns	ns	ns
Inferoapical	ns	*	ns	*	ns	ns
Inferolateral	†	*	ns	*	†	*
Posterolateral	*	*	ns	ns	ns	ns

	Planar left lateral view					
	Comparison of two curves (p-value)					
Anatomic region	Tl vs. Mibi	Tl vs. Tetro	Tl vs. Furi	Mibi vs. Tetro	Mibi vs. Furi	Tetro vs. Furi
Anterobasal	ns	†	†	*	†	*
Anterior	†	†	†	†	†	*
Apical	ns	ns	†	ns	†	ns
Inferior	ns	ns	ns	ns	ns	ns
Posterobasal	ns	ns	ns	ns	ns	ns

*$p < 0.05$; †$p < 0.01$.
Tl = ^{201}Tl; Mibi = ^{99m}Tc-sestamibi; Tetro = ^{99m}Tc-tetrofosmin; Furi = ^{99m}Tc-furifosmin; ns = not significant.

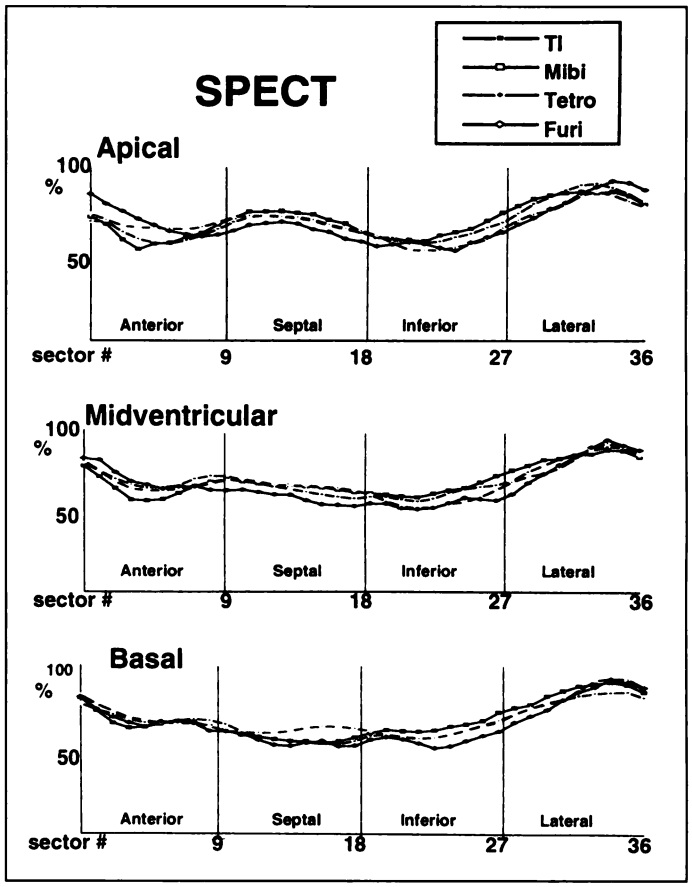

FIGURE 5. Lower-limit-of-normal curves of four radiopharmaceuticals in SPECT apical, midventricular and basal regions. There was no statistically significant difference among the curves of various radiopharmaceuticals (see text).

Nonparametric statistical tests were used throughout because the data usually, but not always, satisfied the underlying assumptions (e.g., normality) required in parametric tests (i.e., ANOVA and t-tests).

Differences among the lower-limit-of-normal curves of each radiopharmaceutical were statistically analyzed by the nonparametric Kruskall-Wallis test. Subsequently, when an overall difference was present at the $p < 0.05$ level, the anatomic segmental location of difference was analyzed using the nonparametric Wilcoxon test. This procedure was done to guard against multiple subgroups tests that would inflate the Type I (false-positive) error rate when there is no overall difference. All reported p values are of the two-sided type.

RESULTS

Visual Characterization of Lower-Limit-of-Normal Curves

Representative planar and SPECT images of normal subjects with various radiopharmaceuticals are shown in Figures 2 and 3.

The lower-limit-of-normal curves of each individual radiopharmaceutical showed general similarities (Figs. 4 and 5). Common characteristics of planar lower-limit-of-normal curves can be described as follows;

Planar-Anterior. The curves show two shallow peaks, one in the septum and one in the anterolateral wall. The shallow valley between the two peaks represents the apical segment. The curves decrease symmetrically at the base of the heart.

Planar-Left Anterior Oblique. The curves show two peaks, one in the inferoseptal area and one in the inferolateral area. A shallow valley in the middle of the curve represents the inferoapical area. The curves are lower at the base of the heart.

Planar-Lateral. The curves show a peak in posterobasal segment, and from here there is a gradual decline from inferior to the anterobasal segment.

SPECT. The curves of relative tracer distribution are similar for SPECT apical, midventricular and basal short-axis slices. The highest peak of the curve is in the lateral segment, there is a second lower peak in the (antero)septal segment. Two shallow valleys occur in the inferior and anterior segments. The curve of the basal slice has only one peak in the anterolateral segment and a shallow valley in the inferoseptal segment.

Statistical Comparison of Lower-Limit-of-Normal Curves

Planar. Comparison of the entire curves using the nonparametric Kruskall-Wallis test revealed significant differences between the curves in the planar left anterior oblique view and in the planar left lateral view ($p < 0.05$ for each). In the planar anterior view no statistically significant differences among the lower-limit-of-normal curves were detected (Fig. 4).

SPECT. No statistically significant differences at the $p < 0.05$ level among the lower-limit-of-normal curves were detected in either the apical, midventricular or basal SPECT short-axis slices (Fig. 5). There was, however, a trend towards significance in some of the SPECT curve comparisons ($0.05 < p < 0.10$). In particular, there were marginally significant differences between the ^{99m}Tc-tetrofosmin and ^{99m}Tc-furifosmin midventricular curves between the ^{99m}Tc-sestamibi and ^{99m}Tc-furifosmin midventricular curves, and between the ^{99m}Tc-tetrofosmin and ^{99m}Tc-furifosmin basal curves.

Segmental Analysis of Lower-Limit-of-Normal Curves

Since there was no statistical difference between the entire curves on the planar anterior view and on the SPECT slices, it was considered statistically inappropriate to submit these curves to further segmental analysis because of the multiple comparisons problem that result in inflation of the overall Type I (false-positive) error rate. Segmental analysis of the planar left anterior oblique and planar left lateral views using the nonparametric Wilcoxon test revealed significant differences among various radiopharmaceuticals. On the left anterior oblique view (Table 2), the most extensive significant segmental difference existed between ^{201}Tl and ^{99m}Tc-tetrofosmin and ^{99m}Tc-sestamibi in four and three anatomical segments, respectively. On the left lateral view (Table 2), the most extensive segmental differences existed between ^{201}Tl and ^{99m}Tc-furifosmin and between ^{99m}Tc-sestamibi and ^{99m}Tc-furifosmin.

DISCUSSION

The results of the present quantitative comparative analysis of normal data files, derived with different radiopharmaceuticals for exercise myocardial perfusion imaging, indicate statistically significant differences between normal planar data files but not between normal SPECT data files. Statistical differences between planar lower-limit-of-normal curves were not only observed between ^{201}Tl and ^{99m}Tc-tracers but also among various ^{99m}Tc-labeled tracers. The most likely explanation for this finding is the differential effect of extracardiac radiopharmaceutical accumulation on acquisition, processing and quantification of planar and SPECT images.

In planar image acquisition, substantial extracardiac activity is superimposed on the heart image. Planar images are quantified using interpolative background subtraction (*16,20*). Interpolative background subtraction is an imperfect empirical algorithm, designed to correct for scatter and cross-talk in the myocardium from adjacent organs (*20*). Initially designed for ^{201}Tl, the algorithm was modified for use with ^{99m}Tc-sestamibi (*16*). Although this modification appeared to perform reasonably well in routine clinical planar imaging, it is based upon empirical adjustment and not on the exact measurements of true background and crosstalk. In addition, other possible causes for the observed differences should be considered for example:

1. Differences in physical properties of ^{201}Tl and ^{99m}Tc-labeled tracers, such as degree of attenuation and scatter.
2. Differences in myocardial kinetics.
3. Differences in relative extra cardiac radiopharmaceutical distribution.
4. Differences in imaging protocols.

The effect of intense subdiaphragmmatic activity is most prominent on planar left lateral images. For instance, use of ^{201}Tl results in relative radiopharmaceutical uptake in the anterior and inferior walls nearly equal to that on exercise planar left lateral images. On the latter images, virtually no subdiaphragmmatic radiopharmaceutical activity is present. In contrast, use of ^{99m}Tc-labeled agents results in relative radiopharmaceutical activity in the inferior wall seemingly higher than that in the anterior wall. This is due to scatter from intense radiopharmaceutical accumulation in subdiaphragmmatic organs. As can be seen in Figure 2, in comparison to other ^{99m}Tc-labeled agents, exercise ^{99m}Tc-furifosmin images, in particular, have relatively low anterior wall activity compared to the inferior wall.

In contrast, for SPECT reconstruction, planar projection images are backprojected in space, thereby separating extracardiac activity from the heart without using background subtraction. Filtering is used to enhance signal-to-noise ratio in reconstructed SPECT images. Although filtered backprojection in the presence of extracardiac activity may cause artifactual myocardial perfusion defects, they generally occur only under extreme conditions (*21*).

Few investigators have performed comparative statistical analysis of normal data files of commonly used radiopharmaceuticals. He et al. (*22*) found, in accordance with our results, no statistically significant difference in stress-induced SPECT defect size using either ^{201}Tl or ^{99m}Tc-sestamibi normal data files for quantification. On the other hand, Van Train et al. (*23*) found a trend for similarity between normal limits established with ^{99m}Tc-labeled agents, but they also observed differences compared to those with ^{201}Tl.

Statistical Analysis

Differences between lower-limit-of-normal curves derived with various radiopharmaceuticals can be analyzed using a variety of statistical tests. The data that generated the lower-limit-of-normal curves were usually, but not always, normally distributed based on Wilks-Shapiro's test for normality. Therefore, the Kruskall-Wallis and Wilcoxon tests were used throughout to avoid the reporting of results based on two different statistical testing procedures. Nevertheless, using parametric testing methods, i.e., ANOVA and t-tests, similar statistical results were generally obtained. Since normality of data usually could not be rejected statistically, one might be inclined to interpret the lower-limit-of-normal curves as representing the lower limit of a 95% confidence interval. This is incorrect, however, since the analysis methods used are not intended for setting 95% confidence intervals for the entire curve.

Normal Databases

Normal data files are generated with the purpose of incorporation in computer quantification software and to allow for accurate and reproducible differentiation between normal individuals and patients with coronary artery disease, as well as quantify myocardial perfusion abnormalities. To what extent one aims to generate normal databases for every conceivable clinical situation is to a certain degree a matter of philosophy. One can construct normal data files for: men and women (*24*), women with varying bra sizes, patients with varying body weight, various age-groups, various modes of stress, rest imaging, various radiopharmaceuticals, various imaging protocols, etc. Nevertheless it will be difficult, if not impossible, to provide normal data files for every conceivable clinical variable.

Furthermore, one can consider whether 1, 2 or 2.5 s.d. below mean radiopharmaceutical uptake provides improved accuracy. In the present study, we compared normal data files generated from good quality images after exercise of men and women without definite attenuation artifacts. We intentionally did not separate male and female files since breast artifacts are often variable and unpredictable (*25*). We consider computer quantification an important and essential aid in image interpretation. Normal data files provide a consistent benchmark against which stress and rest images are compared quantitatively. This objective information enhances confidence and reproducibility of interpretation. Artifacts due to breast attenuation and diaphragmmatic attenuation are better recognized by consistent and disciplined quality control and inspection of planar projection images than by relying on computer quantification.

Study Limitations

In this study, the normal data files were not derived from the same individuals. This may have introduced differences based

upon individual subjects rather than on different radiopharmaceuticals. This limitation, however, may be less important since all individuals were selected using identical criteria for low likelihood of coronary artery disease and conceivably less variation is anticipated within this "normal population." There were differences in imaging protocols for ^{201}Tl and ^{99m}Tc-labeled agents, in particular with regard to the timing of imaging after injection and collimation, that could be responsible for differences in the normal data files. The comparison of normal data files in the present study, however, is of clinical relevance since these are the protocols used in practical clinical imaging. Only exercise normal data files were compared quantitatively. These files are the only relevant files for the detection of stress-induced abnormalities. Rest normal data files generally have larger s.d. and are of relevance for quantitative assessment of defect reversibility. Finally, the number of patients included in each normal data file was relatively small. Although a larger number of subjects obviously would improve statistical reliability, a composite normal data file generally changes only minimally after data of the first 10 normal subjects have been entered.

CONCLUSION

The observations in this study have clinical relevance for visual as well as for quantitative image analysis. Visual interpretation of planar images obtained with different radiopharmaceuticals should take into account substantial differences in the patterns of myocardial uptake. In particular, the effect of extracardiac activity on the image of the normal heart should be considered. Because of demonstrable statistical differences between normal data files of various radiopharmaceuticals, the use of radiopharmaceutical-specific normal data files is mandatory for quantitative analysis of planar images.

On the other hand, use of our imaging protocol and quantification software, revealed great similarity in the visual appearance of SPECT images obtained with different radiopharmaceuticals. No specific adjustment for differences in myocardial uptake pattern is required for visual analysis. Although no statistically significant difference exists between SPECT lower-limits-of-normal curves using our imaging protocol and quantification software, the curves are not identical. Since there was a trend towards significance in some of the SPECT curve comparisons, it also appears prudent to use radiopharmaceutical-specific normal data files for quantitative SPECT imaging.

REFERENCES

1. Wackers FJTh. Comparison of ^{201}Tl and technetium-99m-methoxyisobutyl isonitrile. *Am J Cardiol* 1992;70:30E–34E.
2. Wackers FJTh, Berman DS, Maddahi J, et al. Technetium-99m- hexakis 2-methoxy-isobutyl isonitrile: human biodistribution, dosimetry, safety and preliminary comparison to ^{201}Tl for myocardial perfusion imaging. *J Nucl Med* 1989;30:301–311.
3. Jain D, Wackers FJTh, Mattera J, et al. Biokinetics of ^{99m}Tc-tetrofosmin, a new myocardial perfusion imaging agent: implications for a one day imaging protocol. *J Nucl Med* 1993;34:1254–1259.
4. Gerson MC, Lukes J, Deutsch E, et al. Comparison of technetium-99m-Q12 and ^{201}Tl for detection of angiographically documented coronary artery disease in humans. *J Nucl Cardiol* 1994;1:1499–1508.
5. Beller GA, Watson DD, Ackell P, et al. Time course of ^{201}Tl redistribution after transient myocardial ischemia. *Circulation* 1980;61:791–797.
6. Rosetti C, Vanoli G, Paganelli G, et al. Human biodistribution, dosimetry and clinical use of technetium (III)- 99m-Q12. *J Nucl Med* 1994;35:1571–1580.
7. Wackers FJTh. The maze of myocardial perfusion imaging protocols anno 1994. *J Nucl Cardiol* 1994;1:180–188.
8. Wackers FJTh, Bodenheimer M, Fleiss JL, et al. Factors affecting uniformity in interpretation of planar thallium-201 imaging in a multicenter trial. *J Am Coll Cardiol* 1993;21:1064–1074.
9. Klein JL, Garcia EV, DePuey EG, et al. Reversibility bull's-eye: a new polar bull's-eye map to quantify reversibility of stress induced SPECT ^{201}Tl myocardial perfusion defects. *J Nucl Med* 1990;31:1240–1246.
10. Alazraki NP, Krawczynska G, DePuey EG, et al. Reproducibility of ^{201}Tl exercise SPECT studies. *J Nucl Med* 1994;35:1237–1244.
11. Kaul S, Finkelstein DM, Homma S, et al. Superiority of quantitative exercise ^{201}Tl variables in determining long-term prognosis in ambulatory patients with chest pain: a comparison with cardiac catheterization. *J Am Coll Cardiol* 1988;12:25–34.
12. Iskandrian A, Chae SC, Heo J, et al. Independent and incremental prognostic value of exercise single-photon emission computed tomographic ^{201}Tl imaging in coronary artery disease. *J Am Coll Cardiol* 1993;22:665–670.
13. Marcassa C, Galli M, Temporelli PL, et al. Technetium-99m- sestamibi tomographic evaluation of residual ischemia after anterior myocardial infarction. *J Am Coll Cardiol* 1995;25:590–596.
14. Wackers FJTh. Science, art and artifacts: how important is quantification for the practicing physician interpreting myocardial perfusion studies? *J Nucl Cardiol* 1994;S109–S117.
15. Diamond GA, Forrester JS. Analysis of probability as an aid in the clinical diagnosis of coronary artery disease. *N Engl J Med* 1979;300:1350–1358.
16. Koster K, Wackers FJTh, Mattera J, Fetterman R. Quantitative analysis of planar technetium-99m-sestamibi myocardial perfusion images using modified background subtraction. *J Nucl Med* 1990;31:1400–1408.
17. Wackers FJTh, Fetterman RC, Mattera JA, Clements JP. Quantitative planar ^{201}Tl stress scintigraphy: a critical evaluation of the method. *Semin Nucl Med* 1986;15:46–66.
18. Wackers FJTh, Mattera J. Optimizing planar thallium-201 imaging: computer quantification. *Cardio* 1990;7:103–112.
19. Liu YH, Sinusas AJ, Shi CQX, Shen MYH, Wackers FJTh. Quantification of technetium-99m-sestamibi SPECT based upon mean count improves accuracy for assessment of relative regional myocardial blood flow: experimental validation in a canine model. *J Nucl Cadiol* 1996;3:312–320.
20. Watson DD, Campbell NP, Read EK, et al. Spatial and temporal quantitation of plane ^{201}Tl myocardial images. *J Nucl Med* 1981;22:577–584.
21. Germano G, Chua T, Kiat H, Areeda JS, Berman DS. A quantitative phantom analysis of artifacts due to hepatic activity in technetium-99m myocardial perfusion SPECT studies. *J Nucl Med* 1994;35:356–359.
22. He ZX, Verani MS, Mahmarian JJ. Separate normal patient data banks for thallium-201 and technetium-99m-sestamibi are unnecessary when quantifying perfusion defects with single photon tomography [Abstract]. *J Nucl Med* 1996;37(suppl):178P.
23. Van Train KF, Areeda J, Patterson M, et al. Correlative method for the evaluation of normal distributions in myocardial perfusion SPECT [Abstract]. *J Nucl Med* 1995; 36(suppl):132P.
24. Eisner RL, Tamas MJ, Cloninger K, et al. Normal SPECT thallium-201 bull's eye display: gender differences. *J Nucl Med* 1988;29:1901–1909.
25. Wackers FJTh. Diagnostic pitfalls of myocardial perfusion imaging in women. *J Myocard Ischemia* 1993;14:23–37.